

## EXPERIMENTAL STUDIES OF NON-STATIONARY AERODYNAMIC CHARACTERISTICS OF A HELICOPTER AIRFOIL OSCILLATING IN THE PITCH

Oleg E. Kirillov  
[spintest@Tsagi.ru](mailto:spintest@Tsagi.ru)  
 Head of Department,  
 Ph.D.  
 TsAGI  
 Russia

Nikolay V. Golubev,  
[spintest@Tsagi.ru](mailto:spintest@Tsagi.ru)  
 Leading Engineer  
 TsAGI  
 Russia

Dmitriy A. Petruhin,  
[spintest@Tsagi.ru](mailto:spintest@Tsagi.ru)  
 Engineer  
 TsAGI  
 Russia

Ruslan M. Mirgazov,  
[Ruslan.Mirgazov@Tsagi.ru](mailto:Ruslan.Mirgazov@Tsagi.ru)  
 Head Division, Ph.D.  
 TsAGI  
 Russia

### Abstract

The article presents the results of experimental studies of non-stationary integral and distributed aerodynamic characteristics one of the helicopter airfoil in stationary and non-stationary modes. The stationary mode is a fixed airfoil in a uniform steady airflow. The non-stationary mode is an airfoil oscillating in the pitch in a uniform steady airflow. The investigations were carried out in the vertical, closed-circuit TsAGI wind tunnel with an open test section. The tests were carried out at Reynolds numbers  $Re = 270,000$  and  $540,000$ ; at reduced frequencies from 0.06 to 0.26.

A particular feature of the research was the use of two methods for determining aerodynamic characteristics, namely: a direct method of measuring forces using balance and calculating forces by integrating the pressure distribution along the chord. The obtained results are compared with each other, their satisfactory agreement in the stationary mode is shown.

Another feature of the research was the analysis of pulsations of forces and pressures on the airfoil surface. In particular, using the wavelet analysis, a phenomenon called "frequency explosion", specific of dynamic stall of the flow, is demonstrated.

Keywords: Pitching Airfoil, High Angle of Attack, Dynamic Stall, Wind Tunnel, Wavelet.

### Nomenclature

$C_{xF}$ ,  $C_{yF}$ ,  $mz_F$  – aerodynamics coefficients obtained by direct force measurements;

$C_{yP}$ ,  $C_{xP}$ ,  $mz_P$  – aerodynamics coefficients obtained by integrating the pressure distribution measurements;

$\theta$  – angle of the wing pitch;

$b$  – chord of wing;

$Re$  – Reynolds number;

$A$  – amplitude of the wing oscillations in pitch;

$f$  – frequency of the wing oscillations;

$T=1/f$  – period of the wing oscillations;

$V$  – flow velocity in the wind tunnel;

$k=\pi \frac{bf}{V}$  – reduced frequency;

$C_p$  – pressure coefficient;

$\sigma$  – standard deviation (root mean square).

### 1. Introduction

Dynamic separation of the boundary layer has a decisive influence on the unsteady aerodynamics of the loading surfaces at large angles of attack, in particular on the wings of maneuvering planes, on turbine blades of jet engines and on helicopter's blades.

In the case of helicopters, a dynamic stall occurs on the retreating blades, which operate at large angles of attack to compensate for their low velocities relative to the flow. Such a local stall is one of the sources of vibration of the entire main/tail rotor, can worsen the load of the blades and even cause a phenomenon similar to the instability (stall flutter).

To calculate the characteristics of the main/tail rotor of the helicopter, semi-empirical methods are used, for which experimental unsteady aerodynamic characteristics of the helicopter profile are needed.

Note that for oscillations in the pitch angle, the non-stationary ones are considered to be characteristics corresponding to the reduced frequency greater than 0.05 [1]. Characteristics at lower reduced frequencies are usually called quasi-steady.

Unsteady airloads can be measured using

direct time-resolved force measurements, but this typically requires a dynamic calibration of the force balance system to separate the structural and aerodynamic responses to unsteady aerodynamic forcing. Direct force measurements measure global loads acting on an entire model and do not allow for localization of sources of unsteady loading at specific regions along the chord. Time-resolved (i.e., unsteady) surface pressure measurements, however, provide a means to study the separated (and separating) flow characteristics and can be integrated to determine the impact of the flow features on the unsteady airloads. For example, unsteady surface pressure measurements have been used to study airfoil buffeting and the development of static stall [2], [3]. In these studies, fluctuations in lift and pitching moment were found to be greatest post-stall ( $\alpha=15^\circ$ ) and decrease in magnitude as angle of attack is increased ( $\alpha>20^\circ$ ) [3].

In this paper, the results of measurements of steady and unsteady airloads, both with the help of pressure integration, and with the help of direct measurements of forces and pitching moment are presented.

## 2. Experimental setup

In order to accumulate experimental data on the aerodynamic characteristics of profiles during their unsteady behavior, including the conditions of dynamic stall, the “Dynamic Wing” rig was developed at TsAGI. Wind tunnel tests were performed on a one of a helicopter profile pitching in deep dynamic stall conditions. Figure 1 shows a general view of the wing model with the profile being studied, and Figure 2 is a general view of the wing model on the “Dynamic Wing” rig.

The rig allows testing of models of wings with a chord  $b = 0.1 \dots 0.3$  m and a span of 0.9 m, installed both between the circular plates with a diameter of 0.6 m, and without them. The tests are carried out at the flow velocity in the range  $V = 0 \dots 30$  m/s.

The rig performs static and dynamic tests of the wing model. In dynamic tests, the pitch angle of the wing changes according to the harmonic law:  $\theta = \theta_0 + \cos(\omega t)$ . The oscillation frequency of the wing changes in the range  $f = 0 \dots 10$  Hz, the amplitude of the oscillations is  $0 \dots 10$  degrees. The average pitch of the oscillating wing may vary from 0 to 360 degrees.

Aerodynamic characteristics of helicopter profiles are usually obtained from the pressure distribution measuring results in the section along the surface of the wing model or from the results of determining the aerodynamic forces and moment acting on the weighed compartment

located in the middle part of the tested wing model. In this paper, aerodynamic characteristics of a one helicopter profile are presented for steady  $C_x(\theta)$ ,  $C_y(\theta)$ ,  $m_z(\theta)$  and unsteady  $C_x(\theta(t))$ ,  $C_y(\theta(t))$ ,  $m_z(\theta(t))$  conditions, obtained by both methods and compared. For this, tests were carried out with a wing model equipped with a weighed compartment and installed blocks with pressure sensors to determine the pressure distribution in the section of the wing model.

The axis of oscillations of the wing model and the weighed compartment is located at a distance of 25% of the chord.

The central section of the weighed compartment and the section with drainage holes are located on different sides of the central section of the wing model at a distance up to 100 mm.

Geometrical parameters of the wing model: length 0.9 m, chord 0.2625 m, area 0.236 m<sup>2</sup>, aspect ratio of the wing is 3.44. Geometric parameters of the weighed compartment: length 0.15 m, chord 0.2625 m, area 0.039 m<sup>2</sup>. The determination of the pressure distribution was carried out by means of two units with pressure sensors KDC-24. The total number of points in the section of the wing model is 48: 24 points on the upper surface and 24 points on the bottom surface.

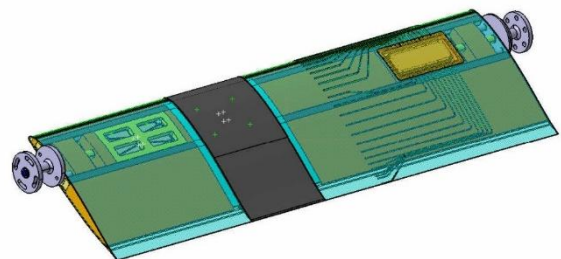


Figure 1: General view of the wing model.



Figure 2: General view of the wing model on the “Dynamic Wing” rig.

The tests were carried out at flow velocities in the wind tunnel  $V = 15 \text{ m/s}$  and  $30 \text{ m/s}$ , which corresponds to the value of Reynolds numbers are  $Re = 270000$  and  $Re = 540000$ . Static tests were carried out at wing's pitch angles varying from  $-6^\circ$  to  $35^\circ$  and back, as well as from  $6^\circ$  to  $-35^\circ$  and back. Dynamic tests were carried out at two amplitudes of wing oscillations  $A = 5^\circ, 10^\circ$  and at frequencies  $f = 2.5$  and  $5.0 \text{ Hz}$ , which corresponded to the reduced frequencies  $k = 0.06, 0.13, 0.26$  at the above flow velocities. The average angles of the wing pitch  $\theta_0$  are  $-25^\circ, -20^\circ, -16^\circ, -15^\circ, -14^\circ, -13^\circ, -12^\circ, -10^\circ, -5^\circ, 0^\circ, 5^\circ, 10^\circ, -12^\circ, -10^\circ, -5^\circ, 0^\circ, 5^\circ, 10^\circ, 12^\circ, 13^\circ, 14^\circ, 15^\circ, 16^\circ, 20^\circ, 25^\circ$  (sequential pass with constant oscillations).

### 3. Results

After processing the force and pressure distribution measurements the following results were obtained.

#### 3.1. Stationary mode

Steady characteristics are  $C_x(\theta)$ ,  $C_y(\theta)$ ,  $m_z(\theta)$  functions of pitch and polar-functions. Fig. 3 shows the wing polar-function  $CyF(CxF)$  from direct measurements and  $CyP(CxP)$  from the pressure distribution measurements. One can see that they are in good agreement, with the exception of the region of minimum values of  $C_x$ , where  $CxP$  exhibits small negative values, which are not accounted for by surface friction when calculating  $C_x$  from the pressure distribution.

In Figures 4 and 5 show graphs of the  $CyF(\theta)$  and  $CyP(\theta)$  for Reynolds numbers  $Re = 270,000$  and  $540,000$ . It can be seen that the difference in coefficients with increasing and decreasing positive pitch angle is the so-called hysteresis effect. The magnitudes of  $Cy$  coefficients are the same for both methods of obtaining them.

Figure 6 shows the graphs  $mzP(\theta)$  and  $mzF(\theta)$  - the moment of the pitch, obtained from direct measurements of forces and from measurements of the pressure distribution. It is clearly seen that they are in a good agreement. Also there is a hysteresis visible at positive angles.

Figures 7 and 8 show the pulsations ( $2\sigma$ ) of the aerodynamic coefficients  $CxF$ ,  $CyF$ ,  $mzF$  at different pitch angles. The conclusions of [3] are confirmed, that pulsations are maximal after the start of detachment and decrease with the further angle increase.

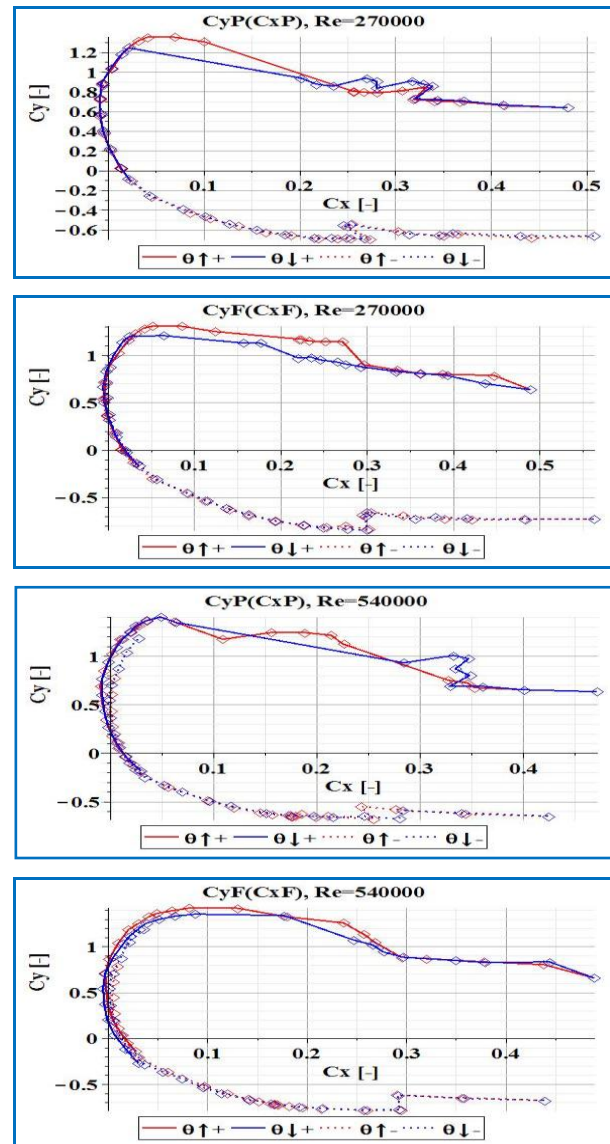


Figure 3.

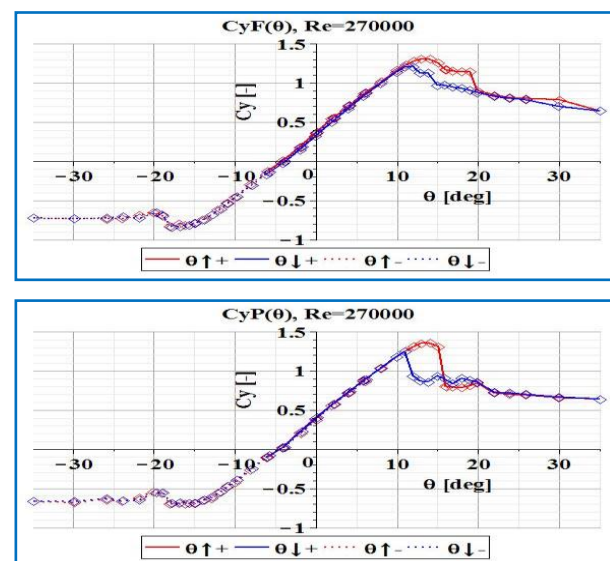


Figure 4.

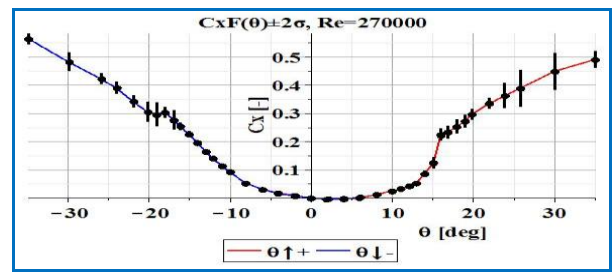
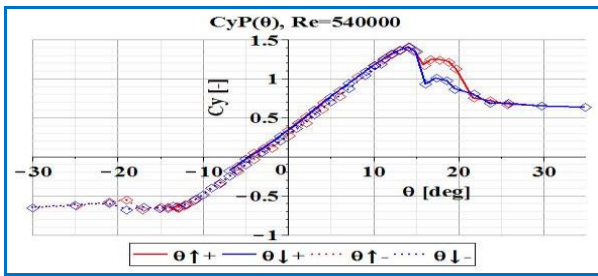
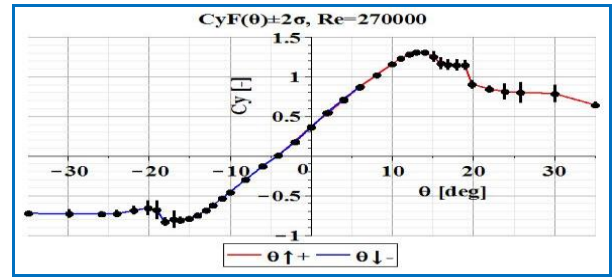
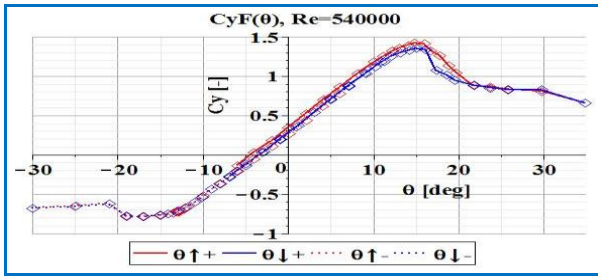


Figure 5.

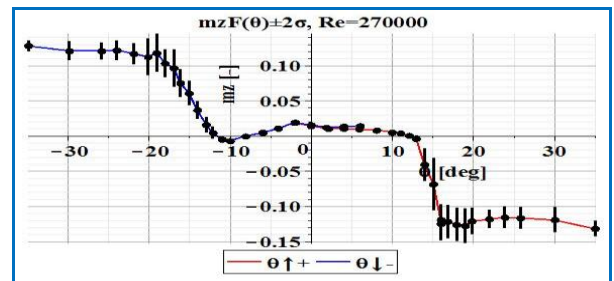
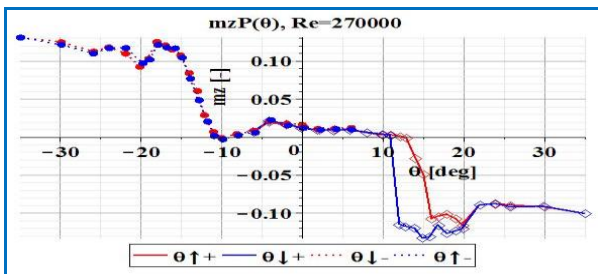


Figure 7.

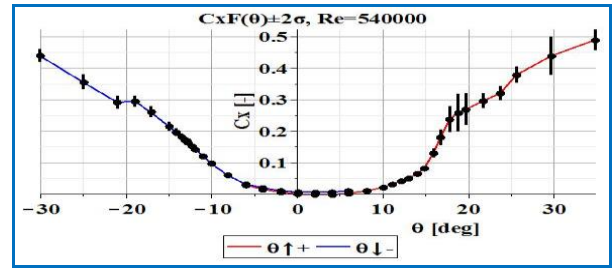
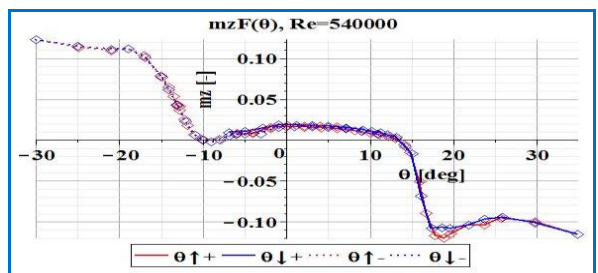
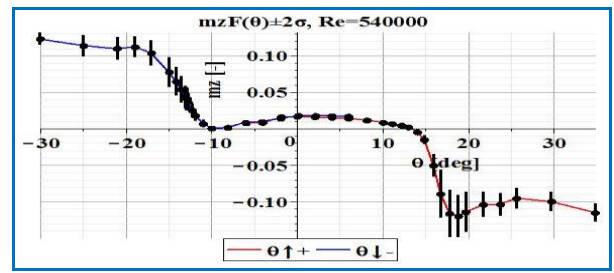
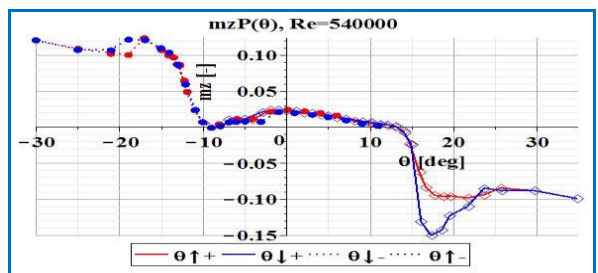
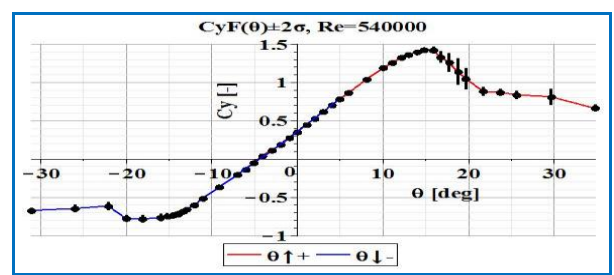
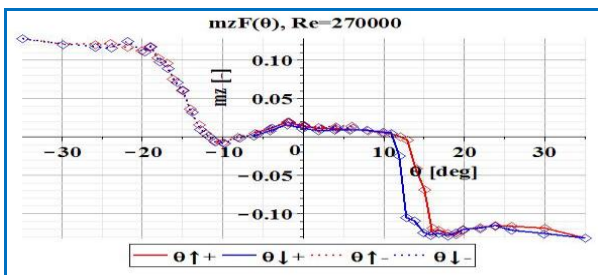


Figure 6.

Figure 8.

The Appendix gives diagrams showing the pulsations ( $2\sigma$ ) of the pressure coefficient  $C_p$  at different points along the airfoil chord. Tables 1A and 2A (Appendix) show the coordinates of the points of the drainage holes for measuring the pressure at the top (Table 1A) and the bottom (Table 2A) of the airfoil surface. Figure 1A and Table 3A correspond to the mode  $Re = 270000$ , mostly positive pitch angles. Figure 2A and Table 4A correspond to the mode  $Re = 270000$ , mostly negative pitch angles. Figure 3A and Table 5A correspond to the mode  $Re = 540000$ , mostly positive pitch angles. Figure 4A and Table 6A correspond to the mode  $Re = 540000$ , mostly negative pitch angles.

### 3.2. Dynamic mode

Dynamic (non-stationary)  $C_x(\theta(t))$ ,  $C_y(\theta(t))$ ,  $C_{mz}(\theta(t))$  aerodynamic characteristics are obtained for the above conditions. Wavelet analysis (using the Morlet wavelet) of time series corresponding to the weight parameters and pressures at the surface points was carried out. The change in the spectral composition of these time series is revealed, in particular, the effect of the "explosion of frequencies" is observed: the appearance on the part of the period of frequency oscillations of the non-multiple frequency of the profile oscillations.

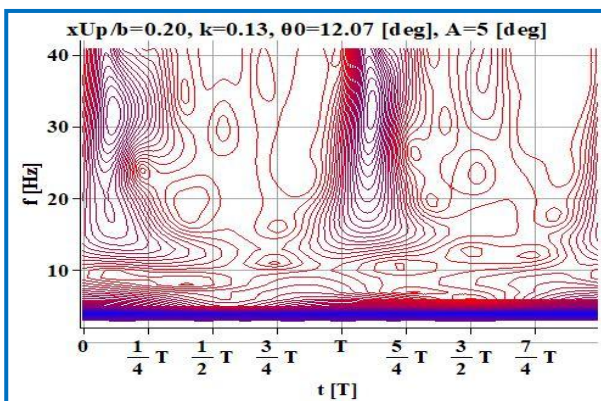


Figure 9

Figure 9 shows a scalogram corresponding to the pressure at the point of the upper surface with the coordinate  $x/b = 0.2$  (the reduced frequency is  $k = 0.13$ , the average pitch angle is  $\theta_0 = 12$  degrees, the amplitude of the oscillations is  $A=5$  degrees), illustrating the effect of the "explosion of frequencies".

The effect of the "explosion of frequencies" is understood as follows. In Figure 9, the red contour-lines are the minimum amplitude of the scalogram, and the blue contour-lines are the maximum amplitudes. It can be seen from the figure that the oscillation frequency ( $f = 2.5$  Hz) is present throughout the period, but in the first quarter of the period, oscillations with frequencies

from 12 to 40 Hz suddenly appear. And the maximum is 30-32 Hz. In the Appendix, Figures 5A-7A show similar diagrams for two points of the upper surface and two reduced frequencies. The diagrams are given both in the format of 2-D contour-lines, and in 3-D diagram format, on which the amplitudes are normalized to the maximum value. It should be specially noted that at  $t = \{0, T, 2T, \dots\}$  the pitch angle assumes the maximum value.

## 4. Conclusions

As a result of experimental studies of the wing model with a helicopter profile in stationary and dynamic modes carried out in the wind tunnel of TsAGI, the following results were obtained

- stationary averaged aerodynamic coefficients  $C_x(\theta)$ ,  $C_y(\theta)$ ,  $m_z(\theta)$  obtained by two methods: direct measurement of forces by means of weights and integration of chord pressure distribution measured on the upper and lower surface of the profile using miniature pressure sensors; the good agreement between the values of these coefficients obtained by the two ways indicated above is shown;

- pulsations ( $2\sigma$ ) of the coefficients of forces  $C_x$ ,  $C_y$  and moment  $m_z$  from the results of direct measurements; it is shown that pulsations reaches their maximum immediately after flow separation, and with a further increase in pitch angle, pulsations decreases; the phenomenon of hysteresis of the coefficients at positive pitch angles is detected (there are practically no hysteresis at negative angles);

- pulsations ( $2\sigma$ ) of the pressure coefficients  $C_p$  at different points of the chord are maximal in the region of the leading and trailing edges;

- dynamic mode demonstrates the effect of "explosion of frequencies".

## References

1. Leishman, J.G., 2006. Principles of Helicopter Aerodynamics, 2nd Edition Cambridge Univ. Press, New York, NY, USA.
2. Coe, C.F., Mellenthin, J.A., 1954. Buffeting Forces on Two-dimensional Airfoils as Affected by Thickness and Thickness Distribution. NACA RM A53K24.
3. Mulleners, K., Pape, A.L., Heine, B., Raffel, M., 2012. The dynamics of static stall. In: 16th International Symposium of Laser Techniques to Fluid Mechanics, Lisbon, Portugal.
4. Andrew H. Lind, Anya R. Jones. Unsteady airloads on static airfoils through high angles of attack and in reverse flow. Journal of Fluids and Structures, ISSN: 0889-9746, Vol: 63, Page: 259-279, 2016

Table 1A – X/b coordinates of drainage points of the upper surface of the profile.

#P	1	2	3	4	5	6	7	8	9	10	11	12	13
X/b	1.0	0.96	0.92	0.88	0.85	0.81	0.76	0.70	0.64	0.56	0.49	0.42	0.35
#P	14	15	16	17	18	19	20	21	22	23	24	25	
X/b	0.297	0.245	0.197	0.15	0.12	0.086	0.062	0.042	0.028	0.018	0.0095	0.0029	

Table 2A – X/b coordinates of drainage points of the bottom surface of the profile

#P	1	2	3	4	5	6	7	8	9	10	11	12
X/b	0.94	0.88	0.83	0.76	0.69	0.62	0.55	0.48	0.41	0.34	0.27	0.21
#P	13	14	15	16	17	18	19	20	21	22	23	
X/b	0.17	0.129	0.1	0.076	0.057	0.043	0.033	0.024	0.014	0.008	0.0	

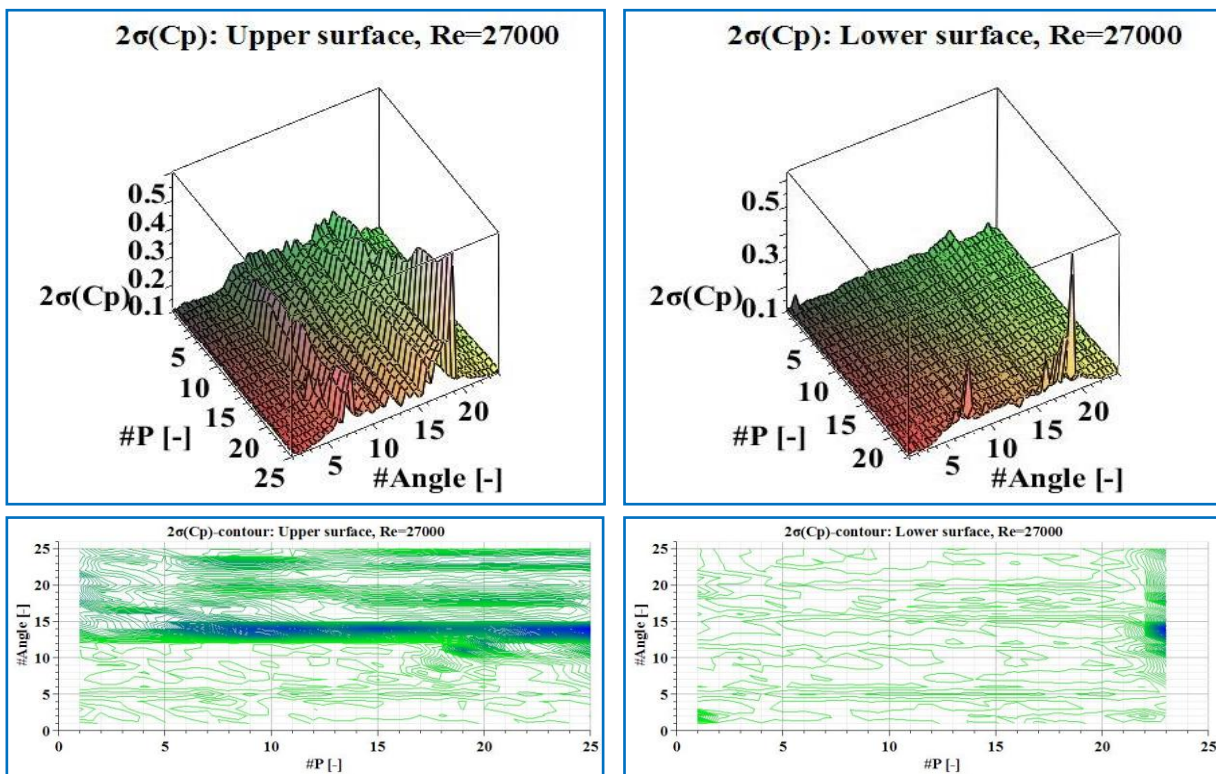


Figure 1A

Table 3A

#Angle θ	1	2	3	4	5	6	7	8	9	10	11	12	13
Angle θ	-6°	-4°	-2°	0°	2°	4°	6°	8°	10°	11°	12°	13°	14°
#Angle θ	14	15	16	17	18	19	20	21	22	23	24	25	
Angle θ	15°	16°	16°	17°	18°	19°	20°	22°	24°	26°	30°	35°	

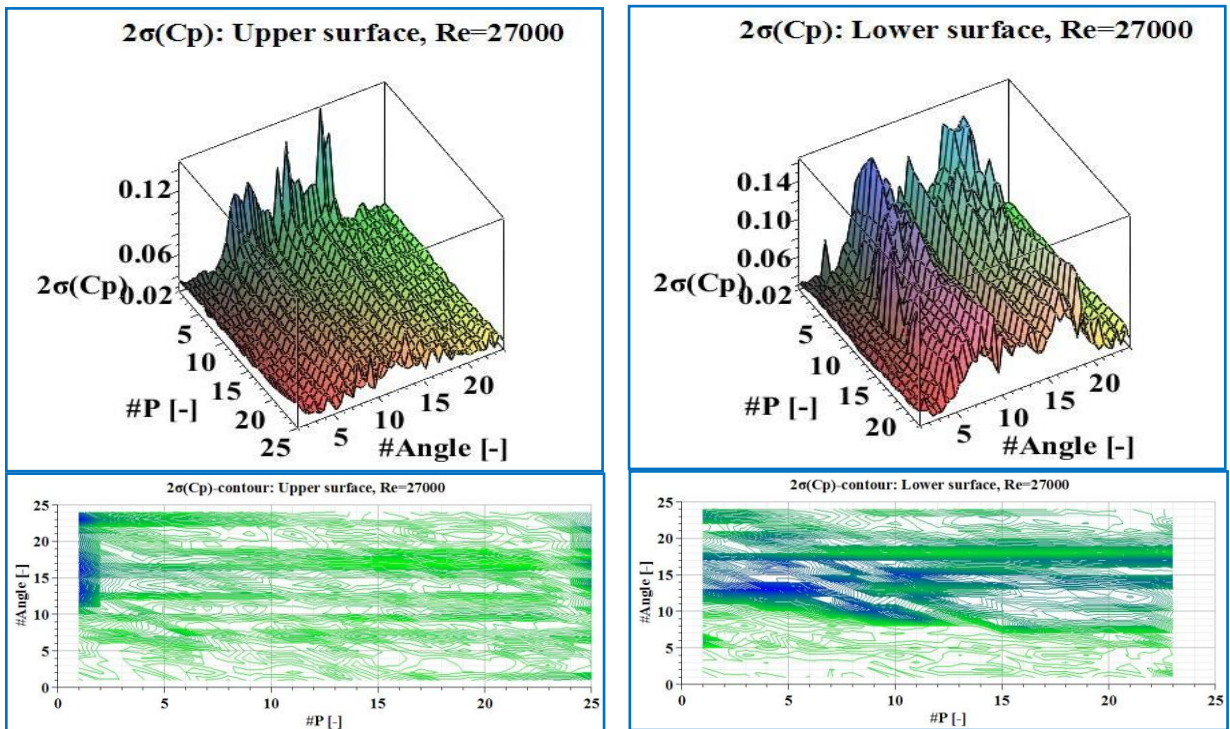


Figure 2A

Table 4A

#Angle $\theta$	1	2	3	4	5	6	7	8	9	10	11	12	13
Angle $\theta$	6°	4°	2°	0°	-2°	-4°	-6°	-8°	-10°	-11°	-12°	-13°	-14°
#Angle $\theta$	14	15	16	17	18	19	20	21	22	23	24		
Angle $\theta$	-15°	-16°	-17°	-18°	-19°	-20°	-22°	-24°	-26°	-30°	-35°		

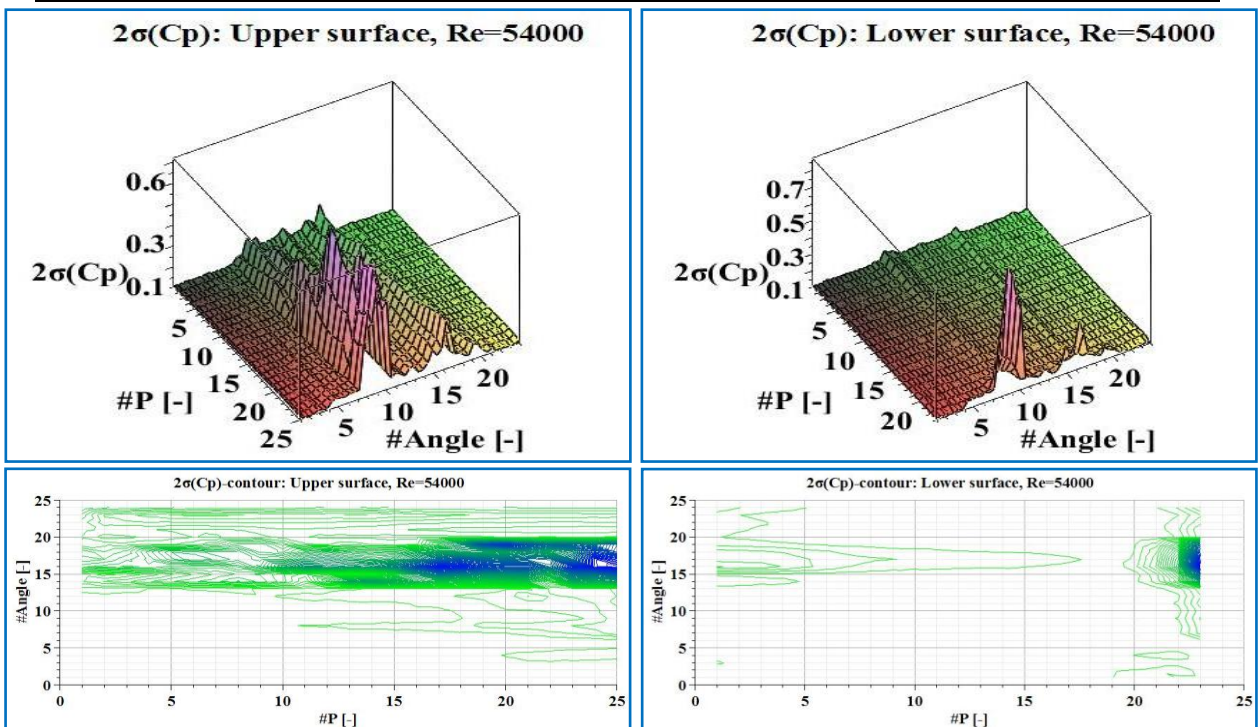


Figure 3A

Table 5A

#Angle $\theta$	1	2	3	4	5	6	7	8	9	10	11	12	13
Angle $\theta$	-6°	-4°	-2°	0°	2°	4°	6°	8°	10°	11°	12°	13°	14°
#Angle $\theta$	14	15	16	17	18	19	20	21	22	23	24		
Angle $\theta$	15°	16°	17°	18°	19°	20°	22°	24°	26°	30°	35°		

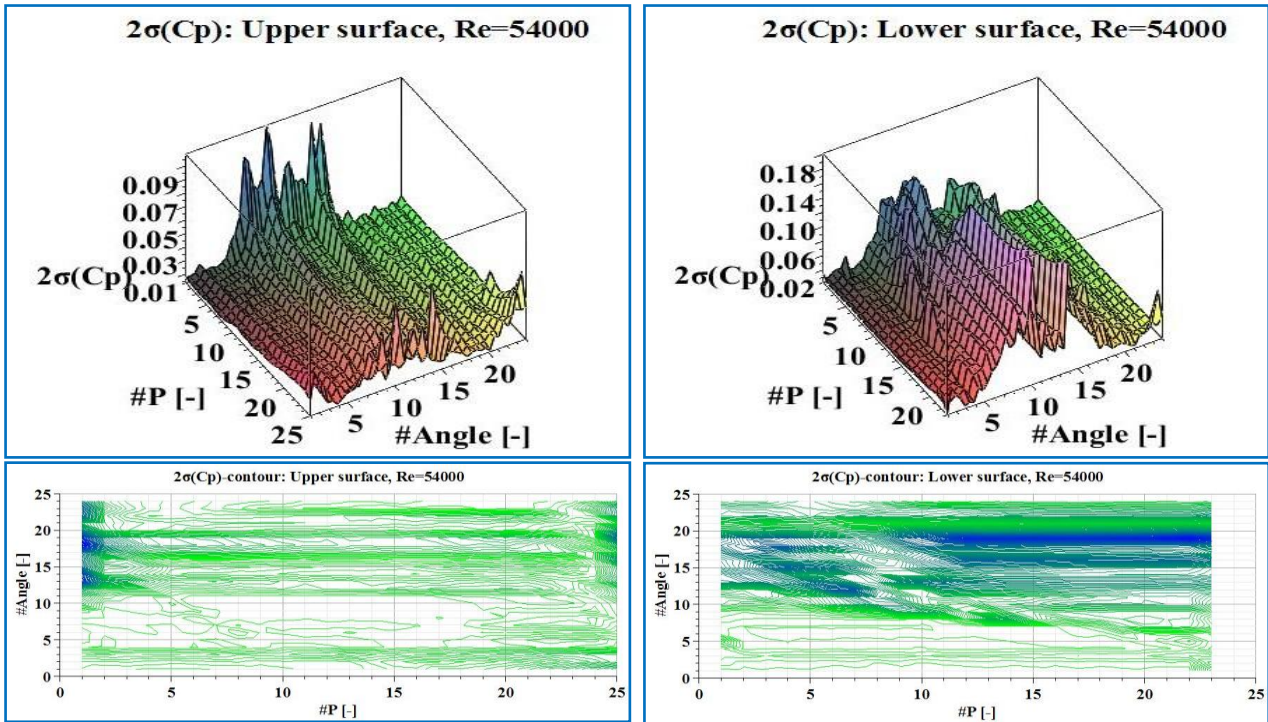


Figure 4A

Table 6A

#Angle $\theta$	1	2	3	4	5	6	7	8	9	10	11	12	13
Angle $\theta$	$6^\circ$	$4^\circ$	$2^\circ$	$0^\circ$	$-2^\circ$	$-4^\circ$	$-6^\circ$	$-8^\circ$	$-10^\circ$	$-11^\circ$	$-12^\circ$	$-13^\circ$	$-14^\circ$
#Angle $\theta$	14	15	16	17	18	19	20	21	22	23	24		
Angle $\theta$	$-15^\circ$	$-16^\circ$	$-17^\circ$	$-18^\circ$	$-19^\circ$	$-20^\circ$	$-22^\circ$	$-24^\circ$	$-26^\circ$	$-30^\circ$	$-35^\circ$		

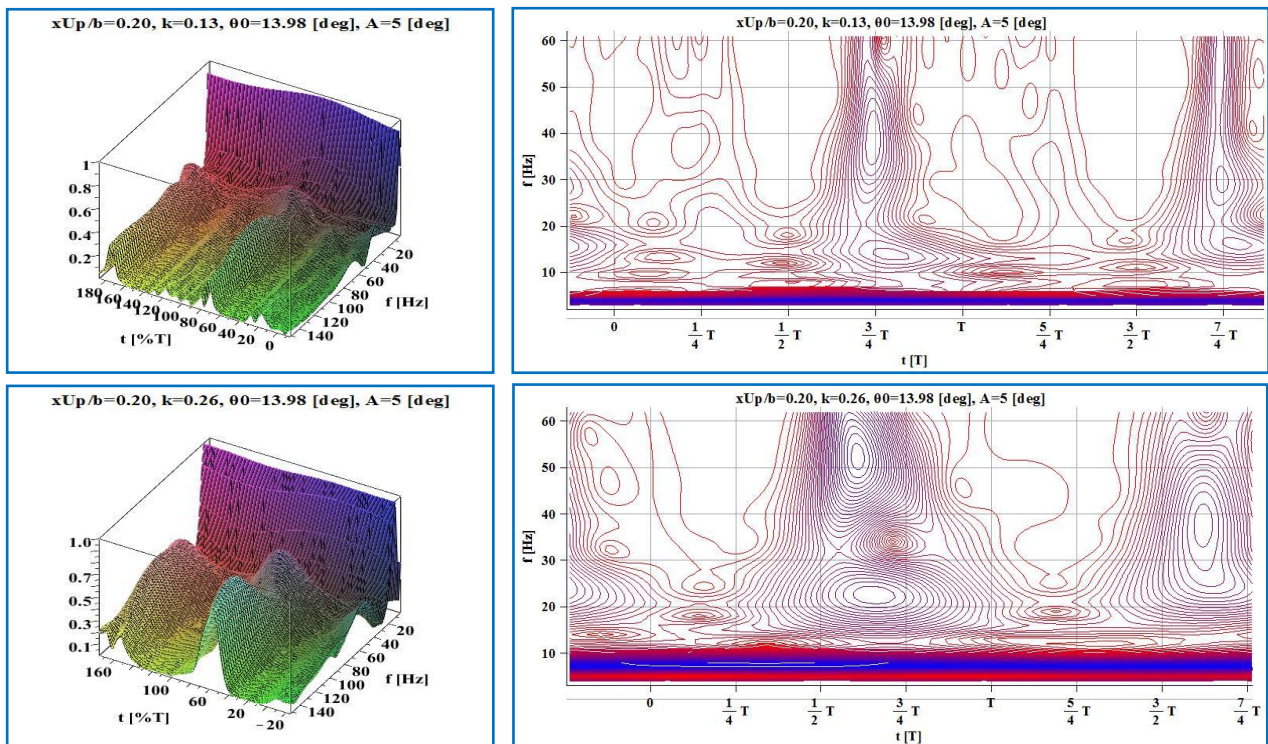


Figure 5A

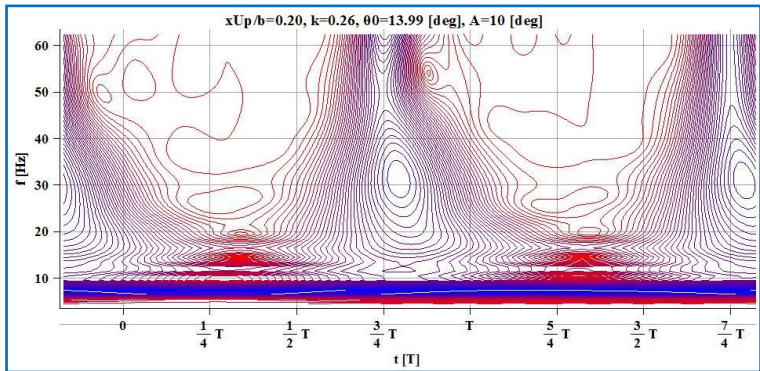
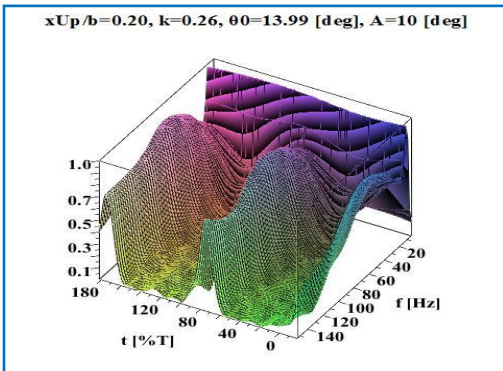
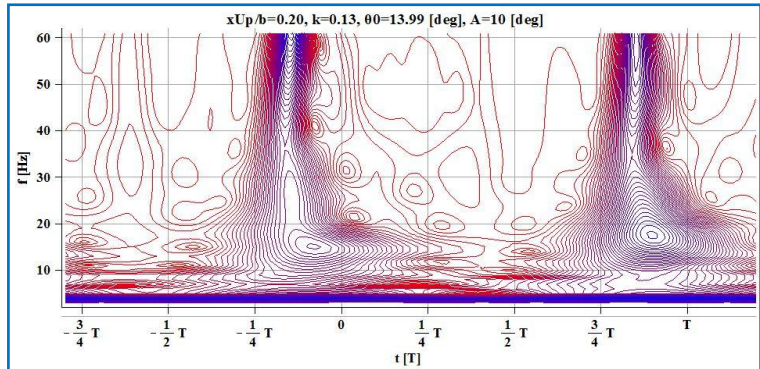
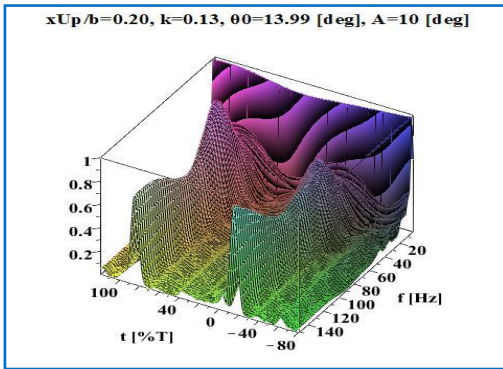


Figure 6A

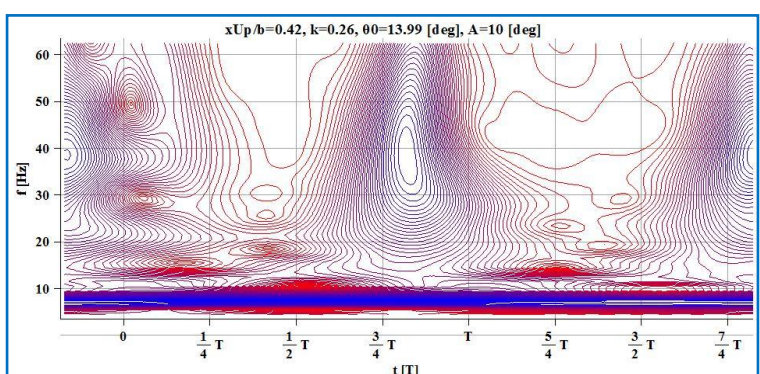
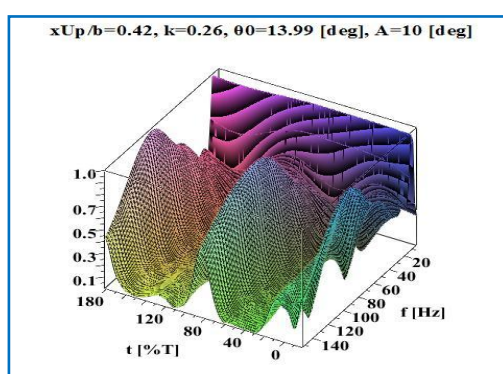
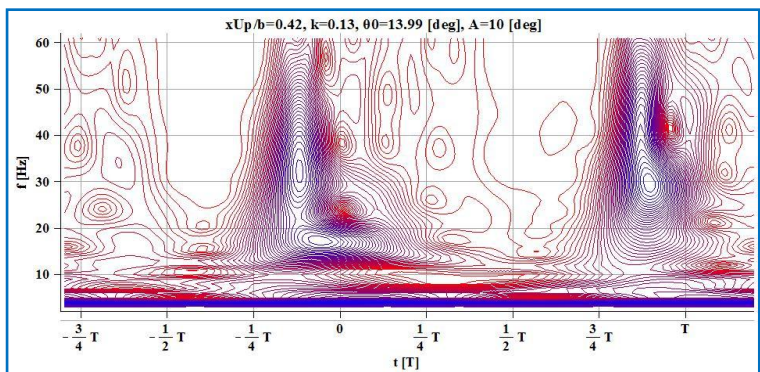
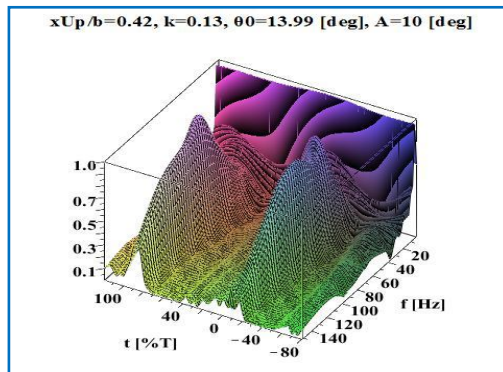


Figure 7A